Multistage vacuum membrane distillation (MSVMD) systems for high salinity applications

Hyung Won Chung, Jaichander Swaminathan, David M. Warsinger, John H. Lienhard V*

Rohsenow Kendall Heat Transfer Laboratory, Department of Mechanical Engineering, Massachusetts Institute of Technology, Cambridge MA 02139-4307 USA

Abstract

Multistage membrane distillation (MD) systems can have significantly higher efficiencies than their single stage counterparts. However, multistage MD system design has received limited attention. In this paper, the performance of a multistage vacuum membrane distillation (MSVMD) which is thermodynamically similar to a multi-stage flash distillation (MSF) is evaluated for desalination, brine concentration, and produced water reclamation applications. A wide range of solution concentrations were accurately modeled by implementing Pitzer's equations for NaCl-solution properties. The viability of MSVMD use for zero liquid discharge (ZLD) applications is investigated, by considering discharge salinities close to NaCl saturation conditions. Energy efficiency (gained output ratio or GOR), second law efficiency, and the specific membrane area were used to quantify the performance of the system. At high salinities, the increased boiling point elevation of the feed stream resulted in lower fluxes, larger heating requirements and lower GOR values. The second law efficiency, however, is higher under these conditions since the least heat for separation increases faster than the system's specific energy consumption with increase in salinity. Under high salinity conditions, the relative significance of irreversible losses is lower. Results indicate that MSVMD systems can be as efficient as a conventional MSF system, while using reasonable membrane areas and for a wide range of feed salinities. Given MD's advantages over MSF such as lower capital requirement and scalability, MSVMD can be an attractive alternative to conventional thermal desalination systems.

Keywords: GOR; second law efficiency; VMD; high salinity; multistage; ZLD; produced water

*Corresponding author: lienhard@mit.edu

Citation: H.W. Chung, J. Swaminathan, D.M. Warsinger and J.H. Lienhard V. "Multistage vacuum membrane distillation (MSVMD) systems for high salinity applications," *J. Membrane Sci.*,497**:128–141, 1 Jan. 2016.

Nomenclature

Roman Symbols

a	Activity
A	Membrane area, m^2
$\overline{A}$	Normalized membrane area
$\widetilde{A}$	Specific area, $m^2/(m^3/day)$
BPE	Boiling point elevation, °C
d	Depth of the feed channel, m
f	Friction factor
g	Specific Gibbs free energy, kJ/kg
h	Specific enthalpy, kJ/kg
h_{fg}	Enthalpy of vaporization, kJ/kg
J	Permeate flux, kg/m^2 s
k_{mass}	Mass transfer coefficient, m/s
M	Molar mass, kg/mol
$\dot{m}$	Mass flow rate, kg/s
N	Number of stages
q	Heat transfer per permeate production, kJ/kg
P	Pressure, kPa
$\bar{r}$	Mean pore radius, µm
Re	Reynolds number
RR	Recovery ratio
T	Temperature, °C
$\dot{V}$	Volumetric flow rate, m^3/day
w	Mass fraction of salts (salinity), %
w_{c}	Width of the membrane module, m
w_{least}	Specific least work of separation, kJ/kg

Greek Symbols

δ	Membrane thickness, µm
ΔT_{f}	Temperature drop of feed in each stage, °C
ΔT_{out}	Excess potential to drive vapor flux, °C
ΔT_{pp}	Pinch point temperature difference, °C
ε	Membrane porosity
η_2	Second Law Efficiency
τ	Membrane tortuosity

Subscripts

0	Environment state
b	Bulk
br	Brine stream
f	Feed stream
in	Inlet
m	Membrane surface
p	Permeate stream
s	Stage

Superscripts

act	Actual system
rev	Reversible system
sat	Saturated state

1. Introduction

Membrane distillation (MD) is a thermally driven desalination technology. In MD, a transmembrane temperature difference establishes a vapor pressure or concentration difference, causing evaporation and vapor transport through the membrane pores. The MD membrane is hydrophobic, and allows only water vapor to pass through, thereby rejecting the passage of the non-volatile solutes in the feed liquid. Depending on the way the transmembrane vapor pressure difference is imposed, there are four major MD configurations: air gap (AGMD), direct contact (DCMD), vacuum (VMD) and sweeping gas (SGMD). Since vapor production is through evaporation rather than boiling, operating temperatures can be lower than the liquid's normal boiling point temperature. As a result, researchers have used several forms of low-grade renewable energy sources, such as solar energy [1, 2, 3, 4, 5, 6] and geothermal energy [7] to run MD systems. Moreover, MD operates at much lower pressures than other membrane desalination technologies such as reverse osmosis (RO). Therefore, the membrane and module housing have much lower mechanical strength requirements and can be constructed out of cheaper materials such as plastics.

MD is considered to be a promising technology for treating highly concentrated saline feed water [8]. It is more resistant to fouling due to its low operating pressure [9, 10] and because only water vapor passes through the membrane pores [11]. Al-Obaidani et al. [12] found that vapor flux decreases only 5% when salinity was varied from 3.5% to 7.5%. Several researchers [8, 13, 14] have proposed and analyzed the use of MD systems for treating produced water from hydraulic fracturing wells, where the feed concentration can be up to five times that of seawater. Mariah et al. [15] investigated the effect of salinity on the flux driving force without considering energy recovery. The effect of salinity on system level efficiency to date is not well understood. Recently, there has been an increasing interest in VMD and hybrids of VMD with other systems, but not many studies have focused on the energy efficiency. Lee and Kim [16] performed a numerical study on hollow fiber multi-stage VMD. Lee et al. [17] studied the the hybrid of multi-stage VMD and pressure retarded osmosis (PRO). But the thermal efficiency was quite low because enthalpy of vaporization was not recycled. Li et al. [18] studied the hybrid of forward osmosis and VMD to treat shale gas drilling flow-back fluid. Hassan et al. [19] proposed a system where the vacuum pump in VMD is replaced with an aspirator to handle incomplete condensation. The gained output ratio (GOR) of a single stage system was limited to less than 1 even with feed preheating. Men et al. [20] compared submerged VMD system with other MD configurations for inland desalination applications.

A comparative study by Summers et al. [21] showed that single stage MD systems typically have low GOR. Although AGMD and DCMD have the potential to achieve high GOR, they require large membrane areas. Summers et al. also showed that the GOR of single stage VMD is limited to being less than 1, even when using extremely large membrane areas because of limitations in the energy recovery process. Higher efficiencies in VMD are possible by multi-staging the system such that the vacuum pressure is progressively lowered for subsequent stages enabling energy recovery at a wide range of condensation temperatures.

Several multistage MD configurations based on DCMD, AGMD and VMD have been designed, focusing

on optimizing overall cost or efficiency. Gilron et al. [22] designed a cascaded DCMD system that was further improved by [23] to increase the recovery. They report GOR in excess of 20, but use low terminal temperature differences for the heat exchangers and DCMD modules (the sum of the terminal temperature difference (TTD) was 2 °C), which would require extremely large areas. We will later show that for high salinity applications, due to the boiling point elevation effect, such a small TTD is impossible, even if one were to use infinite membrane area. Lu et al. [24] modeled multistage AGMD systems and performed cost optimization for operational versus capital costs, and created a flowsheet for determining the optimal path for the cold stream. However, this study lacked GOR or other efficiency analyses. The company memsys has developed a vacuum multi-effect membrane distillation (V-MEMD). The GOR values for this system has been relatively low (less than 4) [25]. A study by Zaragoza et al. experimentally investigated the energy efficiency of several pre-commercial MD prototypes. Of these, multistage configurations are the prototype from Aquaver company which uses V-MEMD modules from memsys and liquid gap MD (LGMD) from Keppel Seghers. They reported a maximum GOR of 3.2 and 2.4 for V-MEMD and LGMD, respectively [26]. Shim et al. [27] developed a multi-VMD system without energy recovery, resulting in a GOR of less than 1. Summers and Lienhard [28] developed a multistage VMD system that is similar to MSF. The condenser heat exchangers were defined based on fixed effectiveness in this model. The absolute temperature difference in the heat exchangers was relatively high, leading to low GORs.

Previous work on multistage MD systems has had low GORs or unreasonably high area requirements. Efficiency, vapor flux and membrane and heat exchanger area requirements need to be considered simultaneously to comprehensively analyze and understand MD system performance. In this paper, we consider all of these metrics to analyze a multistage VMD (MSVMD) system which is thermodynamically similar to well-established multistage flash distillation device (MSF). We also investigate the effect of salinity on GOR, second law efficiency and specific membrane area requirement. Since recovery ratio in a single pass through the system is limited, higher recovery is achieved by recirculating the feed through the system with some brine rejection at the module exit and make-up feed water addition before the feed reenters the module. For crystallization and achieving ZLD operation, brine is rejected close to saturation concentration.

Unlike MSF, MSVMD can be modular, meaning that it can operate on a small scale. Additionally, MSVMD can be constructed with cheaper materials. Therefore, if MSVMD achieves efficiency similar to MSF, it can potentially be attractive for a wide range of applications.

1.1. Similarity between MSF and MSVMD

The similarities between MSF and MSVMD were studied by Summers and Lienhard [28]. They compared the two systems based on GOR and entropy generation analysis. We compare these systems by including the effect of parameters such as salinity, concentration, temperature polarization, and specific membrane area. Figure 1 shows one of the flashing chambers of MSF and a VMD module of MSVMD system along with qualitative T-s digram representations of the processes.

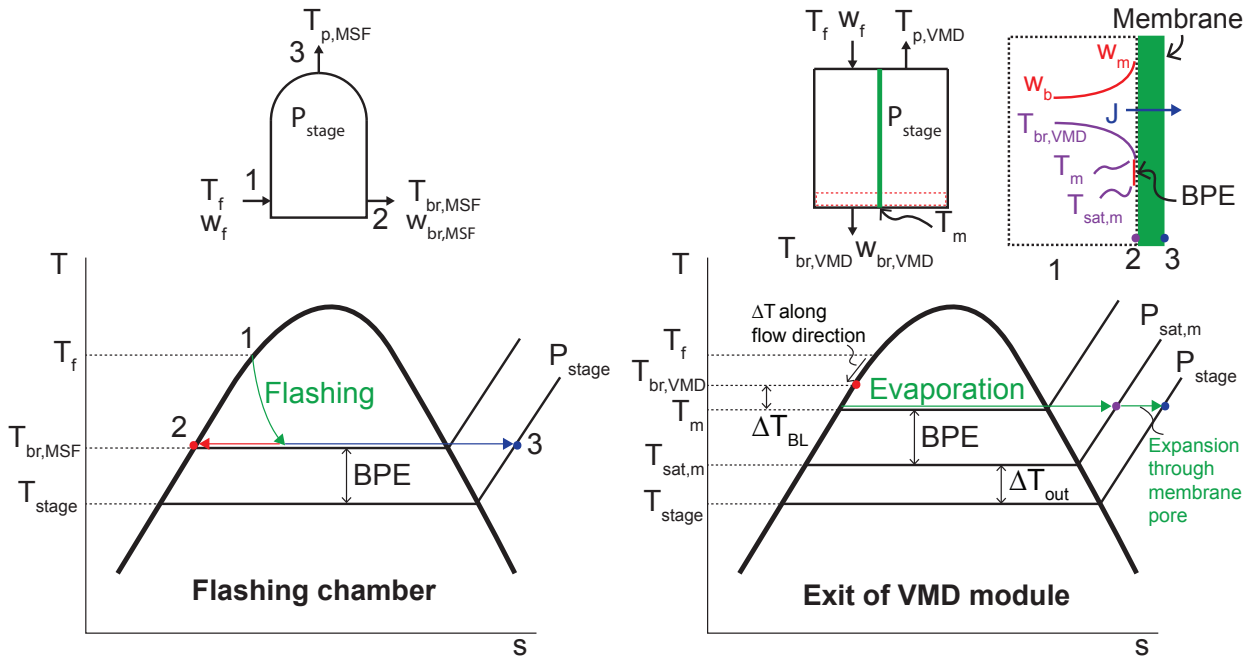

Figure 1: A flashing chamber and a VMD module with same inlet conditions. w is the salinity of NaCl, BL is the boundary layer $T_{\rm sat}$ and $T_{\rm sat,m}$ are saturation temperatures corresponding to $P_{\rm stage}$ and $P_{\rm sat,m}$, respectively.

The same inlet conditions (temperature and salinity of feed) and pressures are maintained in the flashing chamber and permeate side of the VMD module. $T_{\rm stage}$ is pure water's saturation temperature corresponding to the stage pressure. Note that $T_{\rm stage}$ is not the temperature inside the flashing chamber of MSF nor the permeate channel in VMD. The role of $T_{\rm stage}$ is to enable comparison in terms of temperature, rather than pressure. As the feed stream flashes at the inlet of the flashing chamber, its temperature decrease from $T_{\rm f}$ to $T_{\rm br,MSF}$. The temperature inside the flashing chamber is also $T_{\rm br,MSF}$ which is higher than $T_{\rm stage}$ by the boiling point elevation (BPE) as shown in Fig. 1.

An axial temperature distribution exists in the feed channel of VMD because feed stream evaporates at varying temperatures along the flow direction. Therefore, it is not easy to depict the VMD process in a single T-s digram. The T-s digram shown in Fig. 1 describes the process at the exit of the VMD module. The feed stream enters the VMD module at bulk temperature of $T_{\rm f}$ and when it reaches the exit, its temperature is reduced to $T_{\rm br,VMD}$. Water evaporates from the liquid feed at the membrane interface. Then the vapor goes through the membrane pore, which can be modeled as nearly isothermal expansion from $P_{\rm sat,m}$ to $P_{\rm stage}$, as shown in Fig. 1. BPE lowers the effective temperature difference at the membrane surface. $T_{\rm sat,m}$ is defined as the saturation temperature of pure water at the vapor pressure of the feed solution. In other words, when the water vapor at the membrane surface is condensed, its saturation temperature will be $T_{\rm sat,m}$, not $T_{\rm m}$. This temperature characterizes the vapor flux driving temperature difference. In VMD, concentration and temperature polarizations also affect the brine stream's temperature. Temperature close to the membrane surface, $T_{\rm m}$, is lower than the bulk brine temperature, $T_{\rm b}$, by an amount TP and

concentration at the membrane surface is higher than the bulk concentration by CP. The BPE effect in VMD is a function of the concentration at the membrane feed interface rather than the bulk salinity, and hence CP is important. The potential for vapor transfer expressed as a temperature difference is expressed as $\Delta T = T_{\mathrm{b}} - TP - BPE(CP) - T_{\mathrm{stage}}$. In the general case, the brine stream will leave the VMD module with some excess potential to drive vapor flux ΔT_{out}, which is defined as:

$$\Delta T_{\mathrm{out}} = T_{\mathrm{sat,m}} - T_{\mathrm{stage}} \tag{1}$$

Equations 2 and 3 summarize these results,

$$T_{\mathrm{br,MSF}} = T_{\mathrm{stage}} + BPE\left(w_{\mathrm{br}}, T_{\mathrm{br,MSF}}\right) \tag{2}$$

$$T_{\mathrm{br,VMD}} = T_{\mathrm{stage}} + BPE\left(w_{\mathrm{br}} + CP, T_{\mathrm{m}}\right) + TP + \Delta T_{\mathrm{out}} \tag{3}$$

where w_{br} is the brine exit salinity

All the additional terms in Eq. 3 compared to Eq. 2 are positive and they all increase the brine stream's exit temperature. For the same inlet conditions and stage pressure, the brine exit temperature is higher in VMD. Therefore, a smaller amount of permeate will be produced in VMD under the same operating conditions.

As the total membrane area increases, ΔT_{out} decreases. As ΔT_{out} approaches zero, the brine stream leaves the VMD module without much potential to drive flux. Since flux approaches zero, CP, and TP also approach zero. At this condition, the brine exit temperatures from the the flash chamber and the VMD module become equal, and MSVMD stage is almost identical to an MSF stage. It is important to note that this condition requires a significantly large membrane area. In VMD, the main mechanism by which the feed stream loses thermal energy is through evaporation because conduction heat loss through the membrane is negligible. Towards the end of the VMD module, the driving potential for vapor flux exponentially decreases and significantly larger area is required per unit reduction of the feed stream temperature. ΔT_{out} should be a non-zero number for the VMD stage to be practical. Section 3.2 examines the effect of ΔT_{out} on the overall performance of the MSVMD system.

1.2. Performance Metrics

Energetic efficiency of thermal desalination systems is commonly measured in the form of the gained output ratio or GOR, which is defined as:

$$GOR = \frac{h_{\mathrm{fg}}}{q_{\mathrm{in}}} \tag{4}$$

where h_{fg} is the latent heat of vaporization and q_{in} is the specific heat input normalized by the total permeate production. There is no unique choice for the temperature at which h_{fg} is measured. We chose the ambient temperature, T_0 as the reference temperature for GOR. GOR is a measure of how well heat of condensation is recovered within the system. A system that boils water without energy regeneration will have GOR close

to 1 (neglecting heat loss to the environment). Current MD systems typically have low GOR, whereas large scale thermal systems such as MSF might have GOR of 9.5 [29]. In this paper, we show that the GOR of the MSVMD system can exceed 7 for seawater desalination. However, GOR is significantly reduced when brine salinity is higher. GOR alone cannot comprehensively describe the performance under varying salinity conditions.

On the other hand, second law efficiency, η_2, is based on entropy generation or exergy analysis. It is the ratio of theoretical exergy input for a reversible system to the actual exergy input. The exergy of separation for a reversible system can be calculated using a control volume analysis of the black box desalination system shown in Fig. 2. The first and second laws of thermodynamics can be applied to the control volume for which all control surfaces are at ambient temperature. Both work and heat interactions are positive as inputs to the system, and entropy generation is zero for this reversible system. The specific least work ($w_{\text{least}} \equiv \frac{\dot{W}_{\text{least}}}{\dot{m}_{\text{p}}}$) is more relevant than the least work ($\dot{W}_{\text{least}}$). Therefore, the equations can be rearranged for the specific least work (specific least exergy) as [30, 31]:

$$w_{\text{least}} = g_{\text{p}} + \left(\frac{1}{\text{RR}} - 1\right) g_{\text{br}} - \frac{1}{\text{RR}} g_{\text{f}} \tag{5}$$

where RR is the recovery ratio defined as $\text{RR} \equiv \frac{\dot{m}_{\text{p}}}{\dot{m}_{\text{f}}}$, g is the specific Gibbs free energy and subscripts p, br and f refer to permeate, brine and feed, respectively. For a thermal desalination system such as membrane distillation with a heat source temperature T_{H}, least heat of separation is the correct datum to be used in the second law efficiency calculation. Equation 6 shows that how the specific least heat of separation is related to the specific least work of separation through the Carnot efficiency of a cycle operating between T_{H} and T_0:

$$q_{\text{least}} = \frac{w_{\text{least}}}{1 - \frac{T_0}{T_{\text{H}}}} \tag{6}$$

Detailed derivation of the least exergy of separation can be found in Mistry et al. [30]. Equation 7 describes how η_2 is calculated:

$$\eta_2 = \frac{q_{\text{least}}}{q_{\text{act}}} \tag{7}$$

where q_{act} is the actual specific heat input to the system.

Second law efficiency quantifies how close a system operates to the reversible limit. The effect of brine salinity on the reversible heat requirement is considered in this definition. Therefore, both GOR and second law efficiency should be considered for thermal systems that operate over a wide range of salinity conditions.

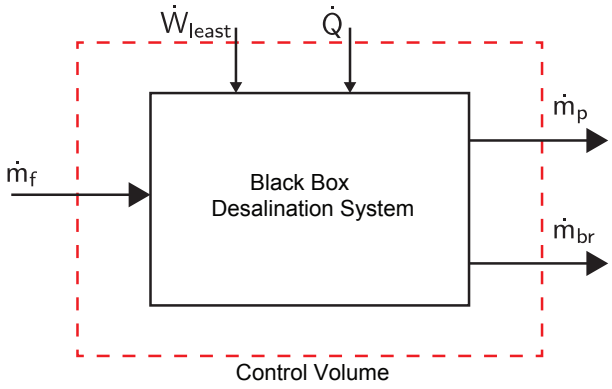

Figure 2: Black box desalination system and control volume.

While efficiency is an important figure of merit for a a thermal desalination system, the capital cost, influenced by the total membrane area needed is another crucial parameter that governs the system's practical viability. Both GOR and η_2 will be maximized if infinite membrane and heat exchanger area are used; however, this system is far from practical. We define a parameter, $\widetilde{A}$ as the ratio of the total membrane area required to the total volumetric permeate production in units of m^3/day. In this paper, $\widetilde{A}$ is referred as specific membrane area:

$$\widetilde{A} = \frac{A_{\text{total}}}{\dot{V}_{\text{p}}} \tag{8}$$

The unit of $\widetilde{A}$ is $m^2/(m^3/\text{day})$. Division by the total permeate production is important because it signals how efficiently a given membrane area is used to desalinate the saline feed. All three metrics for the MSVMD system should be considered to effectively appraise the system.

2. Model Description

The transport processes in VMD are modeled based on the numerical model developed by Summers et al. [21]. A flat sheet VMD module is discretized into computational cells, one of which is shown in Fig. 3.

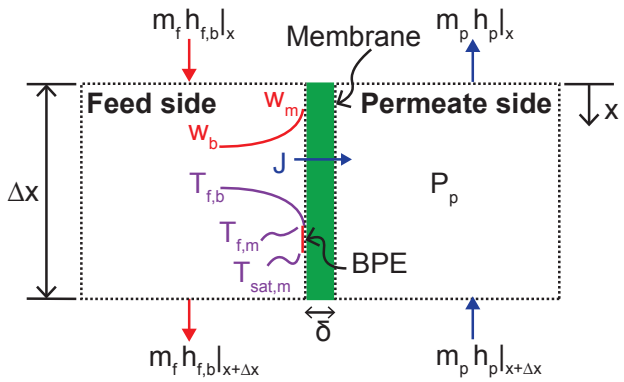

Figure 3: Computation cell used for finite difference simulation.

The mass balance of water and salt, the energy balance equation, and heat transfer correlations constitute the complete set of equations that need to be solved for each computation cell. Interested readers should refer to [21] for a detailed discussion of the modeling approach. In this work, four important features were added to the existing model by Summers et al. [21]: concentration polarization, a more detailed model for mass transfer, a regenerator heat exchanger for the outgoing and incoming streams to improve efficiency, and NaCl solution properties. Nominal values of some input operating conditions are summarized in Table 1.

Table 1: Nominal operating conditions.

Parameter	Value
Feed flow rate, $\dot{m}_{\mathrm{f}}$	15 kg/s
Channel width, w_{c}	0.7 m
Channel depth, d	2 mm
Environment state temperature, T_0	25 °C
First stage's saturation temperature, $T_{\mathrm{stage}}(1)$	77 °C
Last stage's saturation temperature, $T_{\mathrm{stage}}(N)$	35 °C

The membrane modeled is a commercial hydrophobic porous polyvinylidene fluoride (PVDF) membrane with the trade name Durapore (HVHP type), which is supplied by Millipore [32]. Martínez and Florido-Díaz [33] provided a combined geometric factor for the membrane. The membrane's characteristics are summarized in Table 2.

Table 2: Characteristics of Durapore (HVHP) membrane

Parameter	Value
Membrane material	Polyvinylidene fluoride (PVDF)
Pore geometry factor, $\varepsilon/\tau\delta$	3500 m^{-1}[33]
Mean pore radius, $\bar{r}$	0.32 µm [33]

2.1. Mass Transfer Model

In the MD literature, membrane pores are assumed to be cylindrical passages [10]. There are three possible mechanisms of mass transfer that occurs in MD: Knudsen diffusion, molecular diffusion, and viscous flow [9]. In a typical VMD model, molecular diffusion is neglected because the mole fraction of air molecules within pores is assumed to be zero. The Knudsen number is the ratio of the mean free path to the characteristic length scale of the system. Large Knudsen numbers indicate that collisions with the pore walls are more frequent than molecule to molecule collision. In VMD permeate pressure is kept low, which results in a relatively large mean free path as it is inversely proportional to the pressure [10]. In typical VMD operating

conditions, Knudsen numbers vary from 14 to 17 for membrane pore size of 0.2 µm [34]. Therefore, many studies on VMD only consider Knudsen diffusion[35, 34, 27]. In the MSVMD system, vacuum pressure in the initial stages can be high enough that the Knudsen number becomes of order 1. In this case, a viscous flow mechanism should also be included. In this simulation, the Knudsen number is calculated in each computation cell. Matsuura [36] states that Knudsen diffusion is dominant for a Knudsen number greater than 10. The membrane distillation coefficient is calculated as:

$$B = \begin{cases} \frac{2}{3}\frac{\varepsilon\bar{r}}{\tau\delta}\sqrt{\frac{8M_{\mathrm{w}}}{\pi RT}} & \mathrm{Kn} > 10 \\ \frac{2}{3}\frac{\varepsilon\bar{r}}{\tau\delta}\sqrt{\frac{8M_{\mathrm{w}}}{\pi RT}} + \frac{\varepsilon\bar{r}^2}{\tau\delta}\frac{P_{\mathrm{p}}M_{\mathrm{w}}}{8RT\mu} & \mathrm{Kn} \leq 10 \end{cases} \tag{9}$$

where the first term in the Kn ≤ 10 case represents Knudsen diffusion and the second term represents the viscous flow. The vapor flux, J, is calculated using B as:

$$J = B\left(a\left(w_{\mathrm{m}}, T_{\mathrm{m}}\right)P_{\mathrm{m}}\left(T_{\mathrm{m}}\right) - P_{\mathrm{p}}\right) \tag{10}$$

where a is the activity calculated using concentration and temperature at the membrane surface and P_{m} is the saturation pressure of pure water at the membrane surface temperature. For this simulation, the range of Kn was from 0.5 to about 12.

2.2. Concentration Polarization

As water vapor leaves through the membrane, there is a relative increase in local salinity. This increase in salinity creates a concentration gradient (i.e., concentration polarization) which drives diffusion of salt molecules from the membrane surface towards the bulk stream. Fick's law describes this back-diffusion process. Because Summers et al. [21] used thermodynamic properties of pure water, concentration polarization was not considered. In this paper, NaCl solution properties based on Pitzer's equations [37, 38, 39, 40, 41, 42] were implemented in order to capture the concentration polarization and other effects of salinity on the system performance. Since NaCl is the major salt component in many of these saline systems, the properties of the water are approximated as those of a sodium chloride solution of equivalent salinity. For pure water properties, IAPWS-IF97 [43] data was used. The concentration polarization model is the film theory which neglects the convective salt transport along the flow direction within the thin film (the boundary layer) [44]. This approximation is more accurate in turbulent flow because eddies constantly re-establish the concentration boundary layer along the flow direction. Therefore, only turbulent flow was considered in this paper. In practice, turbulent flow may contribute to higher pressure drop. When the flow is changed from turbulent to laminar, the primary effect on thermal efficiency is related to the heat transfer coefficient in the feed channel, which determines the extent of temperature polarization. However, the membrane constitutes the major resistance in the series network of the total resistances. Changing the small thermal boundary layer resistance does not significantly affect the overall transport characteristics of the system. Therefore, the overall thermal analysis based on turbulent flow is similar to that based on laminar flow.

Concentration at the membrane surface is determined by Eq. 11

$$w_{\mathrm{m}} = w_{\mathrm{b}} \exp\left(\frac{J}{k_{\mathrm{mass}}\rho}\right) \tag{11}$$

where J is the vapor flux and k_{mass} is the mass transfer coefficient. The heat and mass transfer coefficients were calculated based on standard heat and mass transfer correlations [45].

2.3. Model Validation

The numerical modeling framework presented above has been validated for pure water by Summers et al. [21]. The effect of dissolved solutes is included in the present model, by using NaCl-water solution properties. The major effect of this change is on the vapor pressure of water which affects vapor transport through the membrane. The model predicts that the flux for a NaCl solution of 26% salinity is 25% lower than that for pure water when the area and the top brine temperature are held constant.

Mericq et al. [46] used VMD to desalinate RO brine solutions (salinity > 5%). Modeling results are compared to the initial flux measurements reported for a wide range of salinity levels (5-30%). For 30% salinity case, this model used 28% salinity because 30% was outside the range of property package. The feed flow rate (characterized by channel Reynolds number), feed temperature and vacuum pressure are also reported and have been used as input conditions for the model.

The channel length and width are equal to 16.5 cm and 3.5 cm and the depth of the channel is 1 mm. The porosity of the membrane is 0.7 [32] and the thickness of the membrane is 175 µm. Mericq et al. [46] reported a Knudsen permeability value of 3.26×10^{-7} s-mol$^{0.5}$/m-kg$^{0.5}$ at 20 °C. From this, tortuosity was calculated as $\tau = 2.9$ using Eq. 9 for the case of Kn>10. While the experiment used RO brine solutions, the model idealizes the feed as a sodium chloride solution of the same total salinity. Since sodium chloride is the major component in seawater and desalination brines, this approximation is quite accurate for estimating the effect of dissolved salt [14].

In this numerical simulation, non-condensable gases were assumed to be absent. In practice, an additional vacuum pump will be used to remove non-condensable gases generated by the evaporation of feed water in each stage (Mericq et al. [46]).

Table 3 shows the results of the model along with the experimental conditions, measured fluxes and modeling results from Mericq et al. [46]. The maximum percent difference from the data is about 15 %. The present model predictions are often closer than those reported in Mericq et al. [46].

Table 3: Comparison between the MSVMD model and the experimental data from Mericq et al. [46]

Feed Salinity	T_f [°C]	P_p [kPa]	Re	J_{exp} [L/hr m^2]	J_{th} Mericq [L/hr m^2]	% difference Mericq	J_{model} [L/hr m^2]	% difference model
5%	53	7	3900	10.1	9.0	-10.9	9.6	-5.1
9.5%	52	5	3800	9.3	9.8	5.4	10.7	14.7
15%	48	4.5	3500	7.9	6.7	-15.2	7.6	-4.1
30%	54	6	3900	7.5	4.5	-40	7.3	-2.1

2.4. Multistage Configuration

Figure 4 is a flow diagram of the MSVMD system. Feed enters the system at 25 °C as make-up water and is sequentially pre-heated by condensation energy released by the permeate stream at each stage. Following this, it flows through an external brine heater which raises the feed temperature to the desired top brine temperature before it enters the first VMD module. After exiting the VMD module, it enters subsequent module whose vacuum side is at a lower pressure. The vacuum pump and feed pump are not shown because energy required for feed circulation and the vacuum pump accounts for a negligible portion of the total energy consumption for VMD [2, 7, 47, 48].

Thermodynamically, the quality of thermal energy is lower than that of electrical energy. The relationship between them is through Carnot efficiency. When a heat source of 100 °C is used with 25 °C environment, the Carnot efficiency is $\eta = 1 - \frac{298}{373} = 0.2$. So exergy of thermal energy is about five times lower than the absolute value of thermal energy. As an example, Wang et al. [48] conducted an experimental study of a solar powered VMD system. For operation from 12:00-14:00 (during this interval, the top brine temperature was around 80 °C), the heating power was around 21 kW and circulation and vacuum pumps consumed 0.37 and 0.18 kW, respectively. Not only is the thermal energy consumption much larger than the electrical energy, but also Carnot efficiency for this solar VMD system is close to unity because the heat source temperature is around 5800 K. Therefore, exergy of electrical energy is small compared to that of thermal energy.

Permeate vapor is produced in each of the VMD modules and it passes into a flashing and mixing chamber where it mixes with the flashed pure water from the previous stages before the combined stream passes into the subsequent heat exchangers. The MD module has an inherently low recovery ratio; therefore, without recirculation, feed pre-treatment costs make the system economically unviable. In steady state, which is the only operation considered in this paper, some portion of brine is recirculated and the rest is rejected. The rejected stream is referred to as a brine blowdown stream. For this study, makeup feed salinity, w_f, and brine blowdown salinity, w_{br} are specified as inputs. For steady state operation, salinity level at the inlet of heat exchanger N, w_{in}, is fixed such that brine blowdown salinity reaches w_{br}. w_f does not affect the steady state operation but determines the proportion of the brine stream that needs to be recirculated. If w_f is higher, a

smaller portion of the brine would need to be recirculated to reach the same value of w_{in}. The mixed stream rejects heat to the cooling water in the brine regenerator.

The pinch point temperature difference, ΔT_{pp}, in the train of heat exchangers usually occurs in heat exchanger 1 in Fig. 4. Although lowering ΔT_{pp} can significantly raise GOR, the heat exchanger area required will be prohibitive. In this study, ΔT_{pp} of 3 °C was specified as an input to represent a practical condenser. It should be noted that ΔT_{pp} does not occur at the outlet of the first heat exchanger. This is because the vapor produced from the VMD module is slightly superheated and water vapor has a lower specific heat than liquid. Therefore, the pinch point occurs where permeate vapor is in the saturated vapor state.

All the permeate side pressures are also set as inputs with the first stage being set to 41.9kPa and the last stage set to 5.6 kPa, corresponding to saturation temperatures of 77 and 35 °C, respectively. In a practical system, heat exchanger size will be fixed and $T_{\text{stage}}(1)$ is determined as an output. However, in the present thermodynamic analysis meant for designing multi-stage VMD systems, $T_{\text{stage}}(1)$ was fixed as an input in order to simplify the heat exchanger analysis. Between the first and last stage, an equal saturation temperature drop per stage is specified, which is typical in MSF system design. By specifying a constant ΔT_{out} in each stage, the feed stream undergoes approximately uniform temperature decreases as it goes through each stage. When the feed stream's salinity varies, boiling point elevation, BPE, changes and the first stage's inlet temperature (i.e., top brine temperature) is adjusted accordingly in order to maintain the uniform temperature decrease and uniform vapor production in each stage.

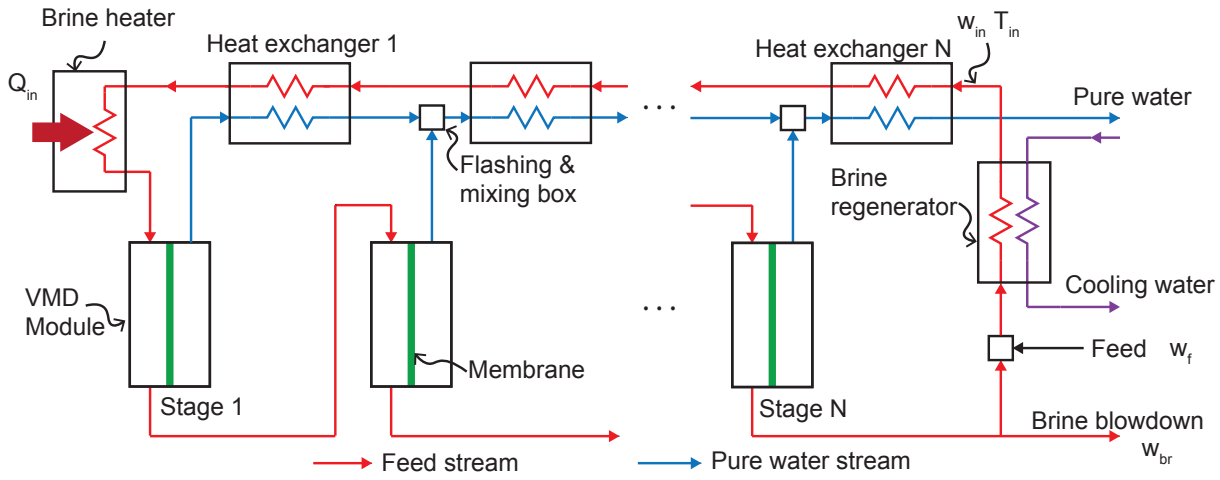

Figure 4: Flow diagram of MSVMD system.

3. Results and Discussion

3.1. Effect of Number of Stages

In this section, the effect of the number of VMD stages on GOR and $\widetilde{A}$ is investigated. The number of stages was varied from 10 to 40 while other parameters were held constant. Although lower vacuum pressure

in the last stage can improve the system, it was limited to 5.63 kPa in this paper. Pressure lower than 5 kPa will require additional effort to maintain vacuum and a lower temperature ambient to condense the vapor that is produced. Three different levels of brine blowdown salinity and ΔT_{out} are considered in order to provide a generic and broad understanding of the system.

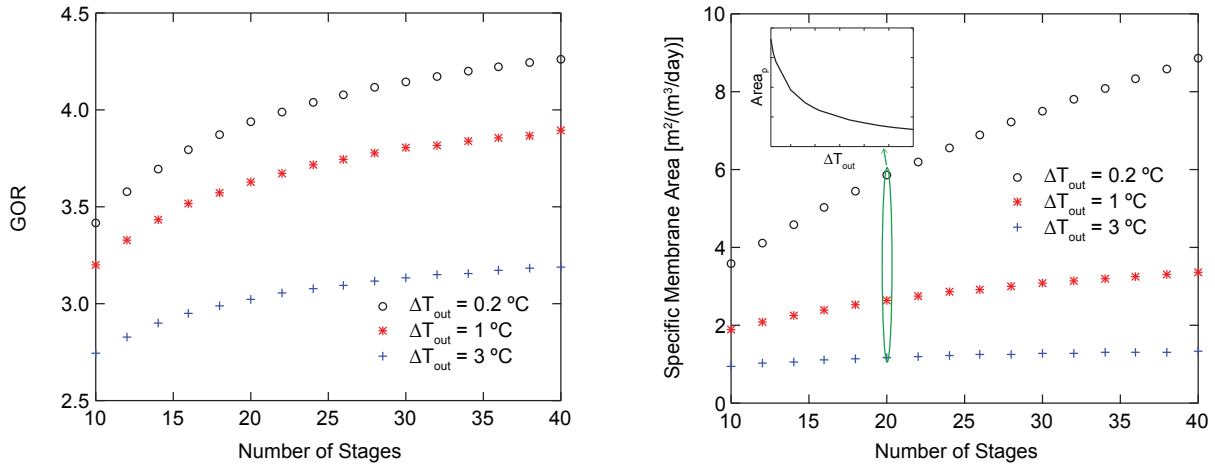

(a) (b)

Figure 5: GOR and the specific membrane area are plotted versus the number of stages. For both cases, brine blowdown salinity is fixed at 26%.

Figure 5a shows GOR as a function of the number of stages for three different levels of ΔT_{out}. The brine blowdown salinity, w_{br}, is 26%. As discussed in Sec. 2.4, w_{in} is determined such that brine blowdown salinity is 26%. For this specific case, w_{in} was about 24.5%. Since the range of pressure (or temperature) is fixed, increasing the number of stages reduces the temperature difference between stages and reduces the temperature change experienced by the feed stream as it goes through each MD stage and the feed heat exchanger. Therefore, the top brine temperature is reduced because a smaller temperature difference is required in the first stage. The top temperature can be expressed as:

$$T_{\text{top}} = T_{\text{stage}}(1) + BPE + TP + \Delta T_{\text{f}} + \Delta T_{\text{out}} \tag{12}$$

where $T_{\text{stage}}(1)$ is the saturation temperature of first stage, TP is temperature polarization and ΔT_{f} is the temperature drop of the feed stream in each stage. The first term on the right-hand side in Eq. 12 is fixed in all cases considered. The second and third terms are roughly the same for the cases with different number of stages. Therefore, reducing ΔT_{f} leads to a reduction in T_{top}. The total permeate production decreases when the number of stages increases. However, the reduction in external heat input decreases at a faster rate, resulting in a overall increase in GOR, albeit at a decreasing rate.

The number of stages affects the specific membrane area as shown in Fig. 5b. As the number of stages increases, the the specific membrane area increases. This trend is more prominent when ΔT_{out} is small.

As the number of stages increases, the temperature decrease of the feed stream in each stage reduces. In other words, the potentials driving the flux at the inlet and at the outlet of each stage become closer to each other, and hence the average temperature difference driving the permeate flux is lower. For small ΔT_{out}, temperature differences that drive flux decrease and become even lower as the number of stages increases. When temperature difference becomes too small, the leverage acquired from the exponential nature of saturation vapor pressure becomes negligible. Therefore, there is a higher penalty for small ΔT_{out} upon increasing the number of stages. When ΔT_{out} is sufficiently large, the specific membrane area increase is more modest as the number of stages increases. However, each new stage will require an additional heat exchanger, adding to capital expenditure. The cost of heat exchangers will therefore limit the number of stages. Another way of interpreting Fig. 5b is to analyze it at one specific value of number of stages. The difference in the specific membrane area increases exponentially as ΔT_{out} decreases. This will be discussed in detail in Sec. 3.2.

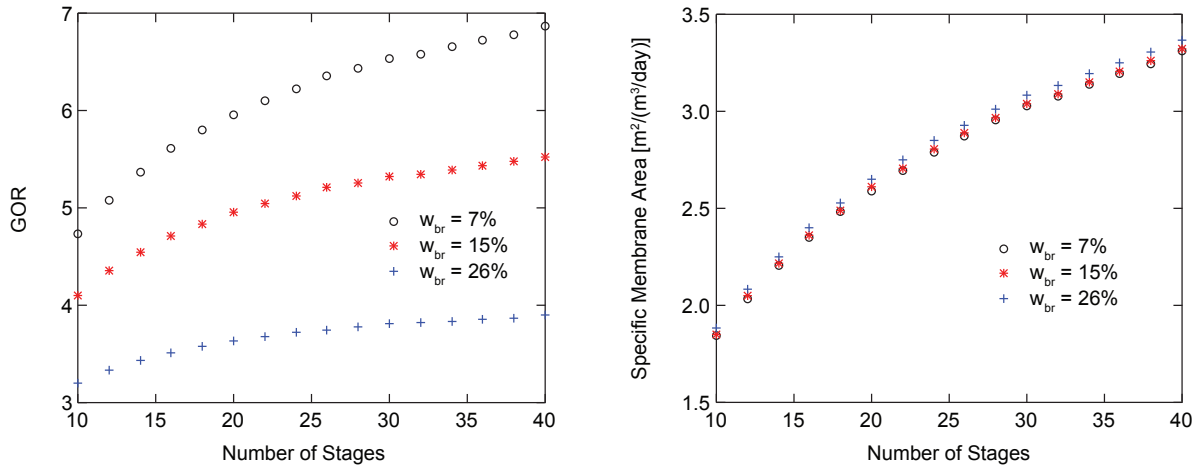

(a) (b)

Figure 6: Effect of number of stages for different levels of brine blowdown salinity. Diminishing returns exist for GOR as vacuum pressure difference between successive stages becomes smaller. For each data set, ΔT_{out} and brine blowdown salinity are fixed.

In order to overcome the higher boiling point elevation, the top brine temperature should be higher when the brine salinity is higher, resulting in larger external heat input. As Fig. 6a shows, GOR is lower when the brine salinity is high, and increasing the number of stages does not significantly improve GOR. Therefore, the number of stages used in the remaining sections is set to 20. Figure 6b shows that the brine salinity has a negligible effect on the specific membrane area. Even though feed bulk temperature is different for three levels of brine reject salinity, vapor flux driving potential is the same because the same ΔT_{out} is imposed in each case.

3.2. *Effect of* ΔT_{out}

In order for MSVMD to be a practically viable system, feed stream has to leave each stage with some potential to drive flux, characterized by ΔT_{out}.

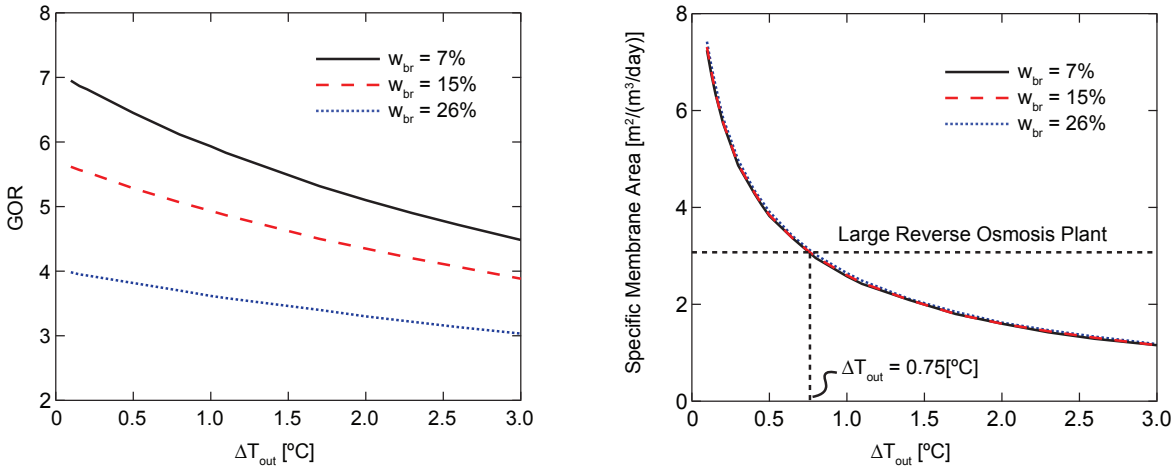

(a) (b)

Figure 7: Effect ΔT_{out} on system performance at 20 stages. Increasing ΔT_{out} drastically reduces the membrane area because flux in MD is driven by transmembrane vapor pressure difference, which increases in exponential function with temperature.

As shown in Fig. 7a, GOR decreases almost linearly. This reduction is mainly due to the boiling point elevation and is discussed in detail in Sec. 3.4. The rate of decline is slower at high salinity because specific heat capacity of feed water decreases with the concentration. So it requires less energy to raise the temperature of higher concentration feed stream. On the other hand, Fig. 7b shows that $\widetilde{A}$ decreases exponentially with increasing ΔT_{out}. Due to its exponential decrease, $\widetilde{A}$ is reduced by a factor of 6 while ΔT_{out} is increased from 0.1 °C to 3 °C. There is a small temperature difference toward the end of each stage. Since flux is driven by a vapor pressure difference which is an exponential function of temperature, the flux level near the exit will be relatively small. Also shown in Fig. 7b is the specific membrane area value (3.1 m^2-day/m^3) of a large scale RO plant [49]. In order for an MSVMD system to have the same specific membrane area, the corresponding ΔT_{out} is about 0.75 °C. For this value of ΔT_{out} and w_{br} of 26%, GOR is 7% lower than the $\Delta T_{\text{out}} = 0$ case, which corresponds the to GOR of MSF due to the similarity described in Sec. 1.1. This result suggests that MSVMD with practical size can be as efficient as MSF, especially at high salinity.

The effect of ΔT_{out} on the specific membrane area is virtually invariant with brine salinity. By forcing the feed stream to leave each stage with a specified potential to drive flux, i.e., ΔT_{out}, almost the same specific area is required regardless of brine salinity. This can be easily visualized by looking at the temperature profiles in the stage.

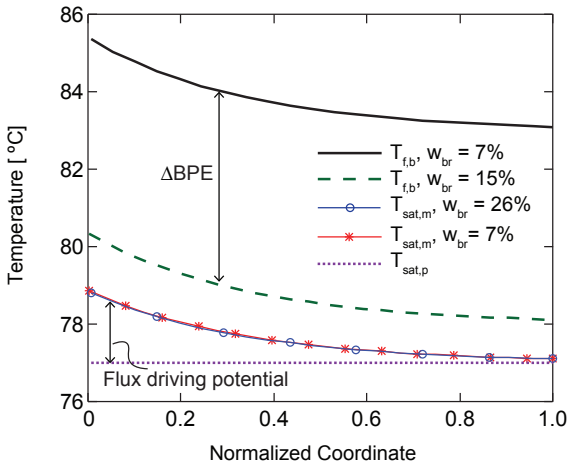

Figure 8: Temperature profiles along normalized coordinates in a VMD stage are plotted. They visually describe the penalty associated with high salinity operation, which is the boiling point elevation.

Figure 8 shows the feed stream's bulk temperature in stage 1 for brine salinity levels of 26% and 7% and $\Delta T_{\text{out}} = 0.1\,^{\circ}\text{C}$ as a function of normalized spatial coordinates along the flow direction; 0 and 1 represent inlet and outlet of the feed channel, respectively. Also shown is the effective flux driving temperature at there membrane surface (i.e., $T_{\text{sat,m}}$) and the saturation temperature corresponding to the permeate pressure. In this model, ΔT_{out} and saturation temperature on the permeate side are fixed. Therefore, the feed stream's bulk temperature is different but the effective flux driving temperature is same for both cases. This is why $\widetilde{A}$ in Fig. 7b is virtually the same regardless of the brine salinity. Figure 8 clearly shows the penalty associated with high salinity operation. The gap between feed bulk temperature curves corresponds to the difference in boiling point elevation of each stream. Boiling point elevation corresponds to the extra temperature rise that the brine heater has to provide.

3.3. Non-uniform Area vs. Uniform Area

In this MSVMD model, ΔT_{out} was used to determine the membrane area. Because of the exponential relationship between saturation vapor pressure and temperature, the membrane area required in each stage becomes a function of temperature. In other words, the same vapor temperature difference across the membrane will not yield the same flux. At higher absolute temperatures, the same difference would yield larger flux than at lower absolute temperatures. Figure 9 shows the membrane area in each stage divided by the rate of permeate production in that stage in units of m^3/day. The membrane area increases exponentially in later stages because absolute temperature is progressively lower.

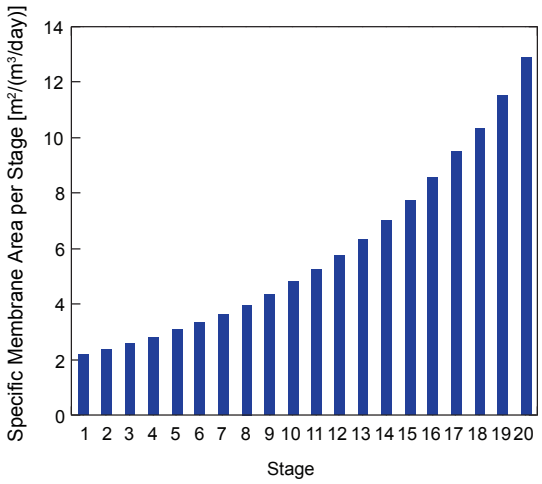

Figure 9: Membrane area of each stage per unit stage permeate production. It increases exponentially at later stages for fixed ΔT_{out} because absolute temperature is lower.

Since temperature drop of the feed stream along the flow direction in each stage was maintained at a constant level through all stages, permeate production in each stage is approximately identical. However, in terms of manufacturing, this design is not desirable as individual VMD modules cannot be mass produced as their sizes are functions of where they will be located within the system. It is easier to manufacture and assemble the system when uniform area is used for all stages. Figure 10 shows how GOR and $\widetilde{A}$ are affected when constant area modules are used for all stages. For this uniform area model, membrane size was not set by explicitly specifying the membrane area in each stage. Therefore, ΔT_{out} is an output of the uniform area model. The rest of the operating conditions such as feed flow rate, operating temperature or salinity are identical to non-uniform area model.

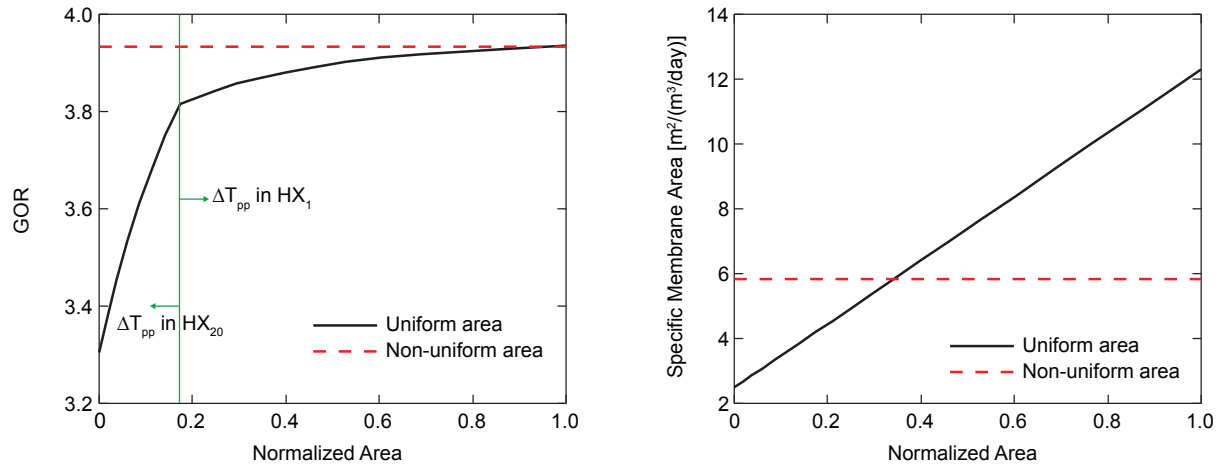

(a) (b)

Figure 10: GOR and specific membrane area as functions of normalized area for uniform area model with 20 stages. Membrane area is normalized relative to the area evaluated in non-uniform area model in Fig. 9 between the lowest (1st stage) and highest (last stage) areas.

Module membrane area is normalized as:

$$\overline{A} = \frac{A - A_1}{A_{20} - A_1} \tag{13}$$

where A_1 refers to the first stage's area in a non-uniform area model, or in Fig. 9, and A_{20} is the largest area used for non-uniform area model. The normalized area varies from 0 to 1 when the smallest and largest area, respectively, are used. According to Fig. 10a, GOR increases at a different rate when the normalized area is increased. After $\overline{A}$ exceeds about 0.17, GOR increases at a much slower rate. A non-uniform area model has highest GOR. To achieve a desired GOR, the non-uniform area model would also use the least specific membrane area as seen in Fig. 10b where the uniform area system achieving similar GOR uses twice the specific membrane area as the non-uniform area system. The non-uniform area model's specific membrane area is equivalent to uniform area model having $\overline{A}$ of about 0.34. At this value of $\overline{A} = 0.34$, this uniform area system's GOR is about 95% of the non-uniform area system. In addition, Fig. 10b shows that $\widetilde{A}$ increases linearly with $\overline{A}$. So extra membrane area does not contribute equally in raising the efficiency. The GOR pattern observed in Fig. 10a is visually explained with temperature profiles of feed and permeate stream in the heat exchanger train in Fig. 11.

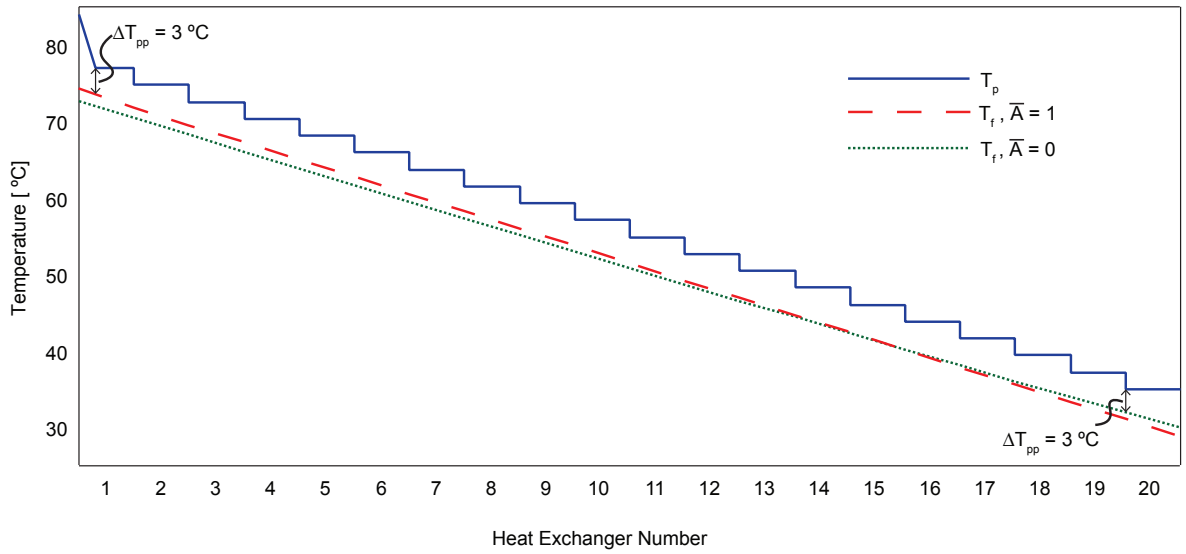

Figure 11: Temperature profiles of permeate stream and feed stream. Feed streams with smallest area and largest area are shown. Pinch point occurs at different locations depending on the membrane area used.

Since the permeate stream is assumed to be pure water vapor, its temperature stays constant within each heat exchanger as it undergoes condensation. The two dashed lines represent temperature profiles of the feed stream as it is heated in the heat exchanger train. The longer-dashed line represents the feed stream when the largest area $\overline{A} = 1$ is used for all 20 stages. The smaller-dashed line uses the smallest area $\overline{A} = 0$. When the largest area is used, more energy is available for regeneration because more vapor is produced. Therefore, temperature of the feed stream increases more in each stage. Because more energy is available, feed streams enter at a slightly elevated temperature, T_{in}. Again, in this model, the smallest temperature difference within the heat exchangers (i.e., ΔT_{pp}) is set at 3 °C, wherever it occurs. For the largest area case, this pinch point occurs at the first heat exchanger. For the smallest area case, on the other hand, the pinch point occurs in the last heat exchanger (i.e., heat exchanger N shown in Fig. 4). It is desirable to have a pinch point in the first heat exchanger because it will lower the external heat input without affecting the permeate production and thus improve GOR. Referring back to Fig. 10a, when the membrane area is increased, GOR starts to increase rapidly. This is because ΔT_{pp} occurs in the last heat exchanger, and increasing the membrane directly affects the temperature with which the feed stream leaves the first heat exchanger. Both reduced heat input and increased permeate production increase GOR. When $\overline{A}$ becomes about 0.17, ΔT_{pp} will occur in the first heat exchanger. From this point on, any further increase in membrane area, or vapor production will not raise the feed stream's exit temperature of the heat exchanger train. So GOR increases at a slower rate only due to extra vapor production. If a uniform membrane area system is preferred, a normalized area of 0.17 appears to be appropriate.

3.4. Effect of Brine Blowdown Salinity

For water concentration applications, the brine blowdown salinity from the MSVMD system is of key interest. The brine blowdown salinity desired can be evaluated knowing the salinity of the feed water and the percentage volume reduction desired by desalination. If disposal costs are high, a larger percentage volume reduction would be desired which would result in a higher w_{br} for the same salinity of the incoming feed (w_{f}).

The recovery ratio or percentage volume reduction possible in a single pass of liquid through the MSVMD system is limited. As a result, to reach higher w_{br} in steady state operation, a part of the brine is recirculated and mixed with the incoming feed water which is then used as the input stream to the MD modules. The salinity of this input stream w_{in}, at steady state, would be chosen such that brine leaves the last stage at the desired value of w_{br}.

Figure 12 shows that GOR decreases as the brine blowdown salinity increases. This graph is independent of w_{f}, as w_{in} is constant for a given w_{br} and the value of w_{f} only influences what fraction of the brine is recirculated and disposed to reach this value of w_{in}. When the MD modules operate at higher feed salinity, due to the higher boiling point elevation of the feed stream, more heat input is required in the heater and less pure water is produced leading to a lower GOR.

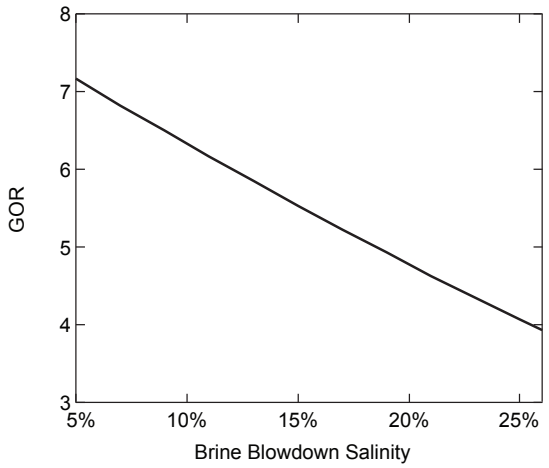

Figure 12: GOR as a function of brine blowdown salinity. GOR decreases linearly with brine blowdown salinity because of increased external heat input. Boiling point elevation represents the penalty of high salinity operation.

A lower GOR corresponds to a higher specific energy consumption by the system. At higher feed or brine blowdown salinities, the specific (per unit production of pure water) least energy consumption for desalination is also higher. The specific least heat consumption for desalination is a function of both the feed and brine salinities. Figure 13a shows the specific least energy consumption at different values of feed and brine blowdown salinities. For a fixed w_{f}, q_{least} increases with w_{br} because q_{least} increases with recovery ratio. However, the magnitude of change in q_{least} is much higher with varying feed salinity, w_{f}, which corresponds

to vertical movement at a specified brine blowdown salinity in Fig. 13a. Thiel et al. [14] found that the specific least work of separation for hydraulic fracturing produced water can be more than five times that for the seawater because w_f for produced water is much higher.

Second law efficiency defined as the ratio of the least heat input necessary to the actual heat input can be used to understand the deviation from ideal behavior. Second law efficiency can take values between 0 and 1, with 1 corresponding to an ideal reversible system. Figure 13b shows the effect of w_{br} and w_f on system second law efficiency. With an increase in brine blowdown salinity at constant feed salinity, the second law efficiency is relatively constant though GOR reduces. This indicates that the increase in specific energy consumption is of the same order of magnitude as the increase in theoretical specific energy required for desalination. On the other hand, second law efficiency is much higher for systems with higher inlet feed salinity. While the actual specific energy consumption and GOR are independent of w_f as discussed previously in this section, the least heat of separation increases significantly leading to higher second law efficiencies. The brine salinity w_{br} determines the operating salinity, and w_f and w_{in} together determine the proportion of recirculation and makeup streams in the brine regenerator. For example, if w_{br} is set at 26% and the seawater is used as a feed stream ($w_f = 35\%$), then w_{in} is determined such that single path will concentrate the brine to 26%. Roughly w_{in} is 24.5%. In this case the minimum theoretical energy consumption should be the least heat of separation corresponding to concentrating seawater to 26%. On the other hand, if the feed stream is produced water from hydraulic fracturing (say $w_f = 15\%$), then w_{in} is still at 24.5% because single path cannot concentrate from 15% to 26%. But the theoretical minimum energy should be the least heat of separation for concentrating produced water from (15% to 26%). In two cases, the proportion of makeup feed stream and recirculated stream are different.

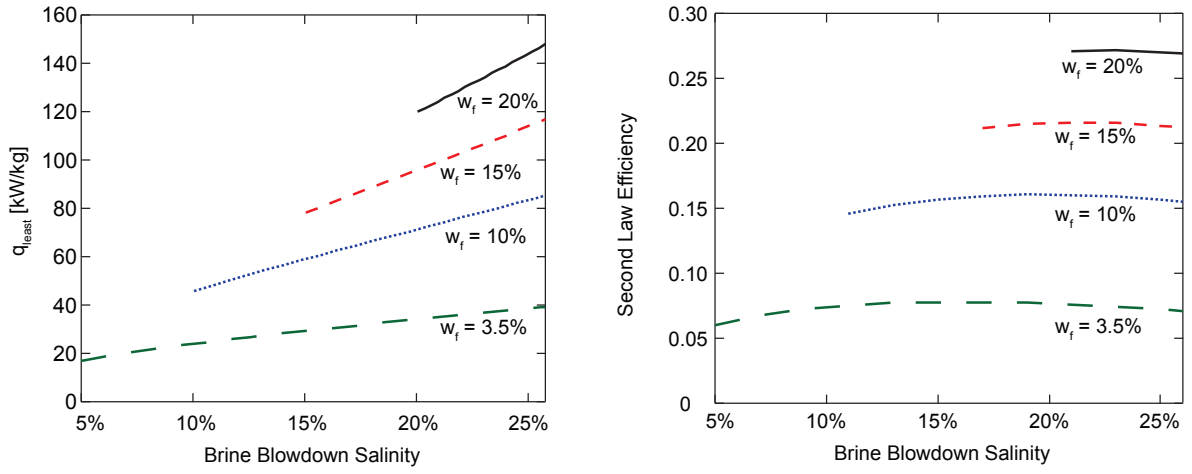

(a) (b)

Figure 13: The specific least heat of desalination and second law efficiency as functions of brine blowdown salinity. Second law efficiency increases with brine blowdown salinity and feed salinity because of increased least heat of desalination.

Figure 14 shows how the second law efficiency is affected when the feed salinity and system component sizes vary. For all data points, the brine blowdown salinity is set at 26%. Figure 14a shows three different values of ΔT_{pp} in the first heat exchanger, corresponding to different sizes of the heat exchangers. Operating conditions for VMD modules are exactly the same regardless of ΔT_{pp} because the top brine temperature is set by the heater and input to the first stage is same. The external heat input is lower at lower ΔT_{pp} leading to a higher second law efficiency because smaller temperature difference in the heat exchanger means lesser extent of irreversibilities. Figure 14b shows the penalty associated with feed exiting each stage with more potential to drive flux. When ΔT_{out} is increased by factor of 15, second law efficiency is reduced by about 30%. A higher value of ΔT_{out} corresponds to a smaller MD membrane area.

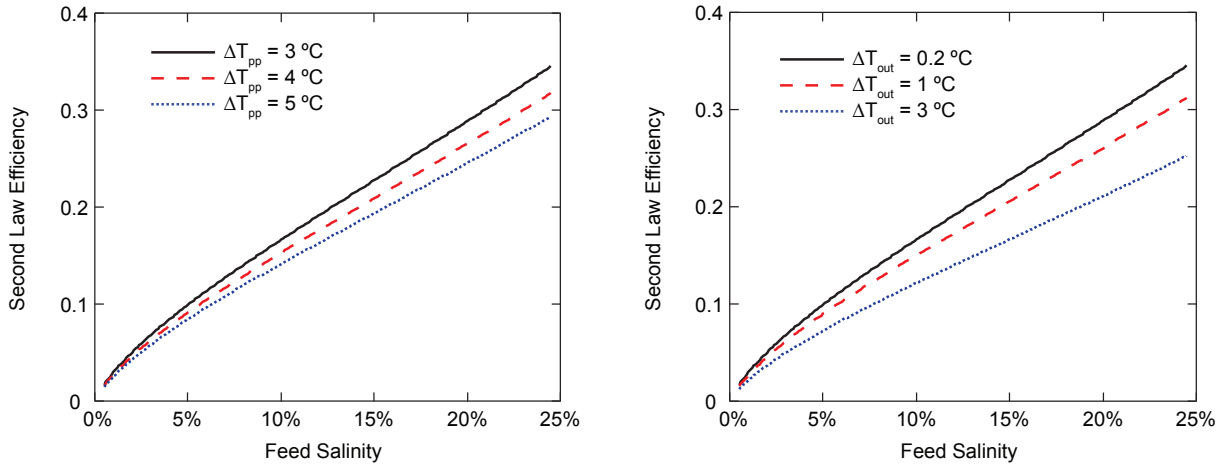

(a) (b)

Figure 14: Second law efficiency as a function of feed salinity. At fixed brine salinity of 26%, external heat input varies less than least heat of separation, so MSVMD operation becomes closer to the reversible limit.

3.5. Effect of Membrane Distillation Coefficient

Currently, there are no commercial membranes specifically designed for MD [11]. In this section, hypothetical membranes with constant membrane distillation coefficient are used to investigate the effect of membrane characteristics on the overall performance of the system.

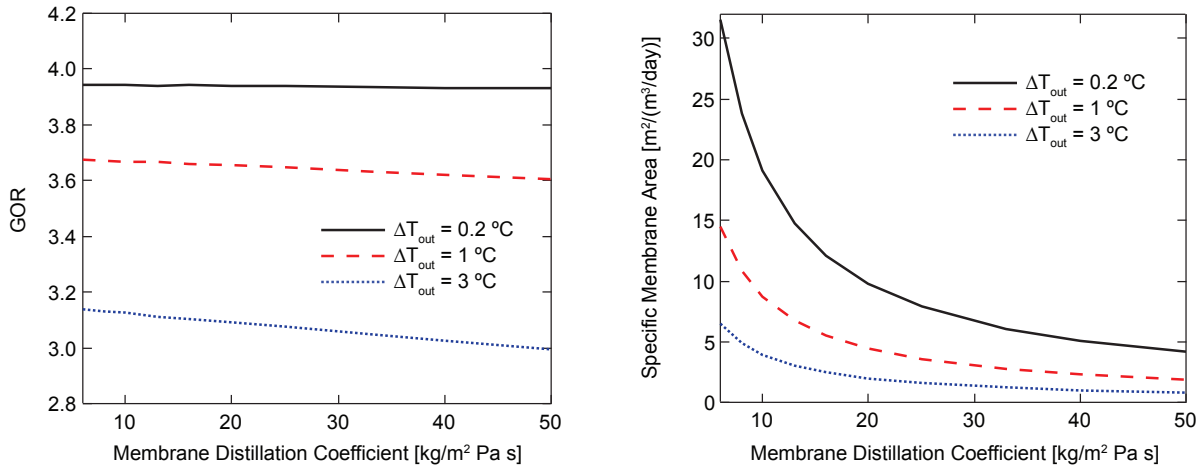

(a) (b)

Figure 15: GOR and specific membrane area as functions of membrane distillation coefficient. For a system with specified ΔT_{out}, a more permeable membrane will slightly reduce GOR because higher flux results in more severe concentration polarization.

For a system defined by ΔT_{out}, GOR depends slightly on the membrane distillation coefficient as shown in Fig. 15a. In this model, conduction heat loss through the membrane is neglected. Therefore, all of the energy decrease experienced by the feed stream is used to evaporate water vapor. The total amount of permeate that can be produced is determined by the total temperature decrease of the feed stream. Higher B value means larger permeate flux for the same driving force. Counterintuitively, Figure 15a shows that GOR decreases slightly when the membrane permeability is higher. This is because of concentration polarization; at high value of B, vapor flux is high, resulting in higher concentration polarization (Eq. 11). Therefore, boiling point elevation at the membrane surface is higher for a more permeable membrane, leading to a higher brine reject temperature (Eq. 3). Thus, a lower total amount of permeate is produced; hence, GOR is lower.

Increasing the permeability of the membrane, quantified by the membrane distillation coefficient B, significantly reduces the membrane area required. For all three values of ΔT_{out}, $\widetilde{A}$ decreases by a factor of about 8 when B is increased from 1 to 50 kg/m^2 Pa s as shown in Fig. 15b.

It should be noted that for a uniform area system, B will affect the system efficiency because higher B means that a given area is used to produce more permeate. However, there exists an upper limit to which B can increase the efficiency. This maximum corresponds to the case when ΔT_{out} approaches zero for that specific B value. At this condition, all the flux driving potential of the feed stream is used such that it is not possible to harness the flux driving potential more effectively. Additionally, at this condition, any increase in area will not produce more flux.

4. Conclusions

Numerical simulations based on the finite difference method were performed to investigate the energetic and exergetic efficiencies and the specific membrane area requirements of an MSVMD system. MSVMD is thermodynamically similar to MSF when a significantly large membrane area is used so that the feed stream leaves each stage without any potential to drive flux. A finite-size MSVMD system was studied by defining ΔT_{out} to force the feed stream to leave with a finite flux-driving potential. In addition, a uniform area system was studied because uniform area stages will be easier to manufacture. A wide range of feed salinities were considered in order to pinpoint the thermodynamic effect of salinity on the MSVMD system and thermal desalination systems in general. The primary conclusions are as follows.

- GOR can be increased by increasing the number of stages. The reason for this increase is that the top temperature is reduced because the temperature drop of the feed stream in each stage is reduced and ΔT_{out} is fixed. This, in turn, reduces the external heat input. However, the lower driving flux in each stage creates rapidly diminishing returns for increasing the number of stages.

- Increasing the flux driving potential with which feed stream leaves each stage (i.e., ΔT_{out}) significantly reduces the specific membrane area requirement with a relatively small sacrifice in GOR. Therefore, MSVMD can be as efficient as MSF with finite membrane size, especially for high salinity operation.

- For a given membrane area, a non-uniform area system is energetically more efficient than a uniform area model. However, it may pose manufacturing difficulties. For uniform-area systems, the location of the smallest temperature difference, i.e., ΔT_{pp}, can be either the first or last heat exchanger depending on the total membrane area and permeate production. Uniform membrane area operations should locate the pinch point in the first heat exchanger in order to maximize GOR.

- For high input feed salinity, the second law efficiency increases because the least heat of separation increases more than the specific external heat input. Also, the second law efficiency is fairly invariant with changes in brine blowdown salinity at constant feed salinity as both specific heat input and least heat of separation increase at similar rates.

- A more permeable membrane will slightly decrease the efficiency of a non-uniform area system where ΔT_{out} is imposed. This is due to the higher concentration polarization caused by higher flux. For a uniform area system, better membranes will increase GOR up to the limit that corresponds to the GOR of a non-uniform area system with ΔT_{out} approaching $0\,^{\circ}\text{C}$.

- For high salinity operation, GOR, second law efficiency, and the specific membrane area requirement should all be considered in order to assess the merits of an MSVMD system. GOR may give a biased picture of the system because it does not account for the increase in theoretical minimum energy of separation. Second law efficiency, while not the most practical metric for efficiency, complements GOR

by taking into account the theoretical minimum exergy. The specific membrane area requirement will dictate the economic viability of the system.

Acknowledgements

The authors acknowledge funding by the Cooperative Agreement Between the Masdar Institute of Science and Technology (Masdar University), Abu Dhabi, UAE and the Massachusetts Institute of Technology (MIT), Cambridge, MA, USA, Reference No. 02/MI/MI/CP/11/07633/GEN/G/00. HC also acknowledges the funding by an MIT Rohsenow fellowship.

We would like to acknowledge Sarah Van Belleghem, McCall Huston, Jocelyn Gonzalez, Priyanka Chatterjee, and Grace Conners for their contributions to this work.

References

[1] P. Hogan, Sudjito, A. Fane, G. Morrison, Desalination by solar heated membrane distillation, Desalination 81 (1–3) (1991) 81 – 90, proceedings of the Twelfth International Symposium on Desalination and Water Re-use. doi:http://dx.doi.org/10.1016/0011-9164(91)85047-X.
URL http://www.sciencedirect.com/science/article/pii/001191649185047X

[2] J. Mericq, S. Laborie, C. Cabassud, Evaluation of systems coupling vacuum membrane distillation and solar energy for seawater desalination, Chemical Engineering Journal 166 (2) (2011) 596 – 606. doi:http://dx.doi.org/10.1016/j.cej.2010.11.030.
URL http://www.sciencedirect.com/science/article/pii/S1385894710011149

[3] J. Koschikowski, M. Wieghaus, M. Rommel, Solar thermal-driven desalination plants based on membrane distillation, Desalination 156 (1–3) (2003) 295 – 304. doi:http://dx.doi.org/10.1016/S0011-9164(03)00360-6.
URL http://www.sciencedirect.com/science/article/pii/S0011916403003606

[4] J. Koschikowski, M. Wieghaus, M. Rommel, V. S. Ortin, B. P. Suarez, J. R. B. Rodríguez, Experimental investigations on solar driven stand-alone membrane distillation systems for remote areas, Desalination 248 (1–3) (2009) 125 – 131. doi:http://dx.doi.org/10.1016/j.desal.2008.05.047.
URL http://www.sciencedirect.com/science/article/pii/S0011916409005761

[5] E. Guillén-Burrieza, G. Zaragoza, S. Miralles-Cuevas, J. Blanco, Experimental evaluation of two pilot-scale membrane distillation modules used for solar desalination, Journal of Membrane Science 409–410 (2012) 264 – 275. doi:http://dx.doi.org/10.1016/j.memsci.2012.03.063.
URL http://www.sciencedirect.com/science/article/pii/S0376738812002645

[6] E. K. Summers, J. H. Lienhard V, Experimental study of thermal performance in air gap membrane distillation systems, including the direct solar heating of membranes, Desalination 330 (2013) 100 – 111. doi:http://dx.doi.org/10.1016/j.desal.2013.09.023.
URL http://www.sciencedirect.com/science/article/pii/S0011916413004554

[7] R. Sarbatly, C. Chiam, Evaluation of geothermal energy in desalination by vacuum membrane distillation, Applied Energy 112 (2013) 737 – 746. doi:http://dx.doi.org/10.1016/j.apenergy.2012.12.028.
URL http://www.sciencedirect.com/science/article/pii/S0306261912009105

[8] D. L. Shaffer, L. H. Arias Chavez, M. Ben-Sasson, S. Romero-Vargas Castrillón, N. Y. Yip, M. Elimelech, Desalination and reuse of high-salinity shale gas produced water: Drivers, technologies, and future directions, Environmental Science & Technology 47 (17) (2013) 9569–9583. arXiv:http://dx.doi.

org/10.1021/es401966e, doi:10.1021/es401966e.
URL http://dx.doi.org/10.1021/es401966e

[9] K. W. Lawson, D. R. Lloyd, Membrane distillation, Journal of Membrane Science 124 (1) (1997) 1 – 25. doi:http://dx.doi.org/10.1016/S0376-7388(96)00236-0.
URL http://www.sciencedirect.com/science/article/pii/S0376738896002360

[10] M. Khayet, T. Matsuura, Membrane Distillation. Principles and Applications, Elsevier, Amsterdam, 2011. doi:http://dx.doi.org/10.1016/B978-0-444-53126-1.10010-7.
URL http://www.sciencedirect.com/science/article/pii/B9780444531261100107

[11] D. M. Warsinger, J. Swaminathan, E. Guillen-Burrieza, H. A. Arafat, J. H. Lienhard V, Scaling and fouling in membrane distillation for desalination applications: A review, Desalination 356 (2015) 294 – 313. doi:http://dx.doi.org/10.1016/j.desal.2014.06.031.
URL http://www.sciencedirect.com/science/article/pii/S0011916414003634

[12] S. Al-Obaidani, E. Curcio, F. Macedonio, G. D. Profio, H. Al-Hinai, E. Drioli, Potential of membrane distillation in seawater desalination: Thermal efficiency, sensitivity study and cost estimation, Journal of Membrane Science 323 (1) (2008) 85 – 98. doi:http://dx.doi.org/10.1016/j.memsci.2008.06.006.
URL http://www.sciencedirect.com/science/article/pii/S0376738808005577

[13] D. Singh, K. K. Sirkar, Desalination of brine and produced water by direct contact membrane distillation at high temperatures and pressures, Journal of Membrane Science 389 (2012) 380 – 388. doi:http://dx.doi.org/10.1016/j.memsci.2011.11.003.
URL http://www.sciencedirect.com/science/article/pii/S0376738811008106

[14] G. P. Thiel, E. W. Tow, L. D. Banchik, H. W. Chung, J. H. Lienhard V, Energy consumption in desalinating produced water from shale oil and gas extraction, Desalination 366 (2015) 94–112. doi:http://dx.doi.org/10.1016/j.desal.2014.12.038.
URL http://www.sciencedirect.com/science/article/pii/S0011916414006857

[15] L. Mariah, C. A. Buckley, C. J. Brouckaert, E. Curcio, E. Drioli, D. Jaganyi, D. Ramjugernath, Membrane distillation of concentrated brines—role of water activities in the evaluation of driving force, Journal of Membrane Science 280 (1–2) (2006) 937 – 947. doi:http://dx.doi.org/10.1016/j.memsci.2006.03.014.
URL http://www.sciencedirect.com/science/article/pii/S0376738806001888

[16] J.-G. Lee, W.-S. Kim, Numerical study on multi-stage vacuum membrane distillation with economic evaluation, Desalination 339 (2014) 54 – 67. doi:http://dx.doi.org/10.1016/j.desal.2014.02.003.
URL http://www.sciencedirect.com/science/article/pii/S0011916414000575

[17] J.-G. Lee, Y.-D. Kim, S.-M. Shim, B.-G. Im, W.-S. Kim, Numerical study of a hybrid multi-stage vacuum membrane distillation and pressure-retarded osmosis system, Desalination 363 (2015) 82 – 91, hybrid Systems for Desalination. doi:http://dx.doi.org/10.1016/j.desal.2015.01.043.
URL http://www.sciencedirect.com/science/article/pii/S0011916415000715

[18] X. Li, B. Zhao, Z. Wang, M. Xie, J. Song, L. D. Nghiem, T. He, C. Yang, C. Li, G. Chen, Water reclamation from shale gas drilling flow-back fluid using a novel forward osmosis-vacuum membrane distillation hybrid system., Water Science And Technology: A Journal Of The International Association On Water Pollution Research 69 (5) (2014) 1036 – 1044.
URL http://libproxy.mit.edu/login?url=http://search.ebscohost.com/login.aspx?direct=true&db=mdc&AN=24622553&site=ehost-live

[19] M. I. Hassan, A. T. Brimmo, J. Swaminathan, J. H. Lienhard V, H. A. Arafat, A new vacuum membrane distillation system using an aspirator: concept modeling and optimization, Desalination and Water Treatment doi:10.1080/19443994.2015.1060902.
URL http://www.scopus.com/inward/record.url?eid=2-s2.0-84931321843&partnerID=40&md5=a930c8a1e37e7d0a447438446ffa1f1f

[20] S. Meng, Y.-C. Hsu, Y. Ye, V. Chen, Submerged membrane distillation for inland desalination applications, Desalination 361 (2015) 72 – 80. doi:http://dx.doi.org/10.1016/j.desal.2015.01.038.
URL http://www.sciencedirect.com/science/article/pii/S0011916415000570

[21] E. K. Summers, H. A. Arafat, J. H. Lienhard V, Energy efficiency comparison of single-stage membrane distillation (MD) desalination cycles in different configurations, Desalination 290 (2012) 54 – 66. doi:http://dx.doi.org/10.1016/j.desal.2012.01.004.
URL http://www.sciencedirect.com/science/article/pii/S0011916412000264

[22] J. Gilron, L. Song, K. K. Sirkar, Design for cascade of crossflow direct contact membrane distillation, Industrial & Engineering Chemistry Research 46 (8) (2007) 2324–2334. arXiv:http://dx.doi.org/10.1021/ie060999k, doi:10.1021/ie060999k.
URL http://dx.doi.org/10.1021/ie060999k

[23] F. He, J. Gilron, K. K. Sirkar, High water recovery in direct contact membrane distillation using a series of cascades, Desalination 323 (2013) 48 – 54. doi:http://dx.doi.org/10.1016/j.desal.2012.08.006.
URL http://www.sciencedirect.com/science/article/pii/S0011916412004365

[24] Y. Lu, J. Chen, Optimal design of multistage membrane distillation systems for water purification, Industrial & Engineering Chemistry Research 50 (12) (2011) 7345–7354. arXiv:http://dx.doi.org/10.1021/ie1016877, doi:10.1021/ie1016877.
URL http://dx.doi.org/10.1021/ie1016877

[25] K. Zhao, W. Heinzl, M. Wenzel, S. Büttner, F. Bollen, G. Lange, S. Heinzl, N. Sarda, Experimental study of the memsys vacuum-multi-effect-membrane-distillation (V-MEMD) module, Desalination 323 (2013) 150 – 160. doi:http://dx.doi.org/10.1016/j.desal.2012.12.003.
URL http://www.sciencedirect.com/science/article/pii/S0011916412006509

[26] G. Zaragoza, A. Ruiz-Aguirre, E. Guillén-Burrieza, Efficiency in the use of solar thermal energy of small membrane desalination systems for decentralized water production, Applied Energy 130 (2014) 491 – 499. doi:http://dx.doi.org/10.1016/j.apenergy.2014.02.024.
URL http://www.sciencedirect.com/science/article/pii/S0306261914001603

[27] S. Shim, J. Lee, W. Kim, Performance simulation of a multi-VMD desalination process including the recycle flow, Desalination 338 (2014) 39 – 48. doi:http://dx.doi.org/10.1016/j.desal.2013.12.009.
URL http://www.sciencedirect.com/science/article/pii/S0011916413005869

[28] E. K. Summers, J. H. Lienhard V, Cycle performance of multi-stage vacuum membrane distillation (MS-VMD) systems, in: IDA World Congress on Desalination and Water Reuse, Tianjin, China, 2013.
URL http://web.mit.edu/lienhard/www/papers/conf/SUMMERS_IDA_Tianjin_2013.pdf

[29] O. A. Hamed, M. A. Al-Sofi, M. Imam, G. M. Mustafa, K. B. Mardouf, H. Al-Washmi, Thermal performance of multi-stage flash distillation plants in saudi arabia, Desalination 128 (3) (2000) 281 – 292. doi:http://dx.doi.org/10.1016/S0011-9164(00)00043-6.
URL http://www.sciencedirect.com/science/article/pii/S0011916400000436

[30] K. H. Mistry, R. K. McGovern, G. P. Thiel, E. K. Summers, S. M. Zubair, J. H. Lienhard V, Entropy generation analysis of desalination technologies, Entropy 13 (10) (2011) 1829–1864. doi:10.3390/e13101829.
URL http://www.mdpi.com/1099-4300/13/10/1829

[31] K. H. Mistry, J. H. Lienhard V, Generalized least energy of separation for desalination and other chemical separation processes, Entropy 15 (6) (2013) 2046–2080. doi:10.3390/e15062046.
URL http://www.mdpi.com/1099-4300/15/6/2046

[32] Http://www.emdmillipore.com/US/en.

[33] L. Martínez, F. Florido-Díaz, Theoretical and experimental studies on desalination using membrane distillation, Desalination 139 (1-3) (2001) 373–379. doi:10.1016/S0011-9164(01)00335-6.
URL http://www.sciencedirect.com/science/article/pii/S0011916401003356

[34] J. Mengual, M. Khayet, M. Godino, Heat and mass transfer in vacuum membrane distillation, International Journal of Heat and Mass Transfer 47 (4) (2004) 865 – 875. doi:http://dx.doi.org/10.1016/

j.ijheatmasstransfer.2002.09.001.
URL http://www.sciencedirect.com/science/article/pii/S0017931003004721

[35] K. W. Lawson, D. R. Lloyd, Membrane distillation. I. module design and performance evaluation using vacuum membrane distillation, Journal of Membrane Science 120 (1) (1996) 111 – 121. doi:http://dx.doi.org/10.1016/0376-7388(96)00140-8.
URL http://www.sciencedirect.com/science/article/pii/0376738896001408

[36] T. Matsuura, Synthetic Membranes and Membrane Separation Processes, CRC Press, Boca Raton, FL, 1993.

[37] K. S. Pitzer, Thermodynamics of electrolytes. I. Theoretical basis and general equations, The Journal of Physical Chemistry 77 (2) (1973) 268–277. doi:10.1021/j100621a026.
URL http://dx.doi.org/10.1021/j100621a026

[38] K. S. Pitzer, J. J. Kim, Thermodynamics of electrolytes. IV. Activity and osmotic coefficients for mixed electrolytes, Journal of the American Chemical Society 96 (18) (1974) 5701–5707. doi:10.1021/ja00825a004.
URL http://dx.doi.org/10.1021/ja00825a004

[39] D. J. Bradley, K. S. Pitzer, Thermodynamics of Electrolytes. 12. Dielectric Properties of Water and Debye-Hückel Parameters to 350° C and 1 kbar, The Journal of Physical Chemistry 83 (12) (1979) 1599–1603.

[40] K. S. Pitzer, J. C. Peiper, R. H. Busey, Thermodynamic Properties of Aqueous Sodium Chloride Solutions, Journal of Physical and Chemical Reference Data 13 (1) (1984) 1–102. doi:10.1063/1.555709.
URL http://scitation.aip.org/content/aip/journal/jpcrd/13/1/10.1063/1.555709

[41] K. S. Pitzer, A thermodynamic model for aqueous solutions of liquid-like density, Reviews in Mineralogy and Geochemistry 17 (1987) 97–142.

[42] J. F. Zemaitis, D. M. Clark, M. Rafal, N. C. Scrivner, Handbook of Aqueous Electrolyte Thermodynamics, Wiley-AIChE, Malden, MA, 1986.

[43] W. Wagner, J. R. Cooper, A. Dittmann, J. Kijima, H. J. Kretzschmar, A. Kruse, R. Mareš, K. Oguchi, H. Sato, I. Stöcker, O. Šifner, Y. Takaishi, I. Tanishita, J. Trübenbach, T. Willkommen, The IAPWS industrial formulation 1997 for the Thermodynamic Properties of Water and Steam, Journal of Engineering for Gas Turbines and Power 122 (1) (2000) 150–184.
URL http://dx.doi.org/10.1115/1.483186

[44] S. Kim, E. M. Hoek, Modeling concentration polarization in reverse osmosis processes, Desalination 186 (1–3) (2005) 111 – 128. doi:http://dx.doi.org/10.1016/j.desal.2005.05.017.
URL http://www.sciencedirect.com/science/article/pii/S0011916405006867

[45] V. Gnielinski, New equations for heat and mass transfer in turbulent pipe and channel flow, Int. Chem. Eng 16 (2) (1976) 359–368.

[46] J. Mericq, S. Laborie, C. Cabassud, Vacuum membrane distillation of seawater reverse osmosis brines, Water Research 44 (18) (2010) 5260 – 5273. doi:http://dx.doi.org/10.1016/j.watres.2010.06.052.
URL http://www.sciencedirect.com/science/article/pii/S0043135410004392

[47] C. Cabassud, D. Wirth, Membrane distillation for water desalination: How to chose an appropriate membrane?, Desalination 157 (1–3) (2003) 307 – 314, desalination and the Environment: Fresh Water for all. doi:http://dx.doi.org/10.1016/S0011-9164(03)00410-7.
URL http://www.sciencedirect.com/science/article/pii/S0011916403004107

[48] X. Wang, L. Zhang, H. Yang, H. Chen, Feasibility research of potable water production via solar-heated hollow fiber membrane distillation system, Desalination 247 (1–3) (2009) 403 – 411. doi:http://dx.doi.org/10.1016/j.desal.2008.10.008.
URL http://www.sciencedirect.com/science/article/pii/S0011916409005220

[49] M. Wilf, L. Awerbuch, C. Bartels, M. Mickley, G. PearcNikolay, Voutchkov, The Guidebook to Membrane Desalination Technology : Reverse Osmosis, Nanofiltration and Hybrid Systems Process, Design, Applications and Economics, Balaban Publishers, Rehovat, Israel, 2011.